# Experiments of mass transfer with liquid–liquid slug flow in square microchannels

Nathalie Di Miceli Raimondi, Laurent E. Prat, Christophe Gourdon, Josiane Tasselli

http://dx.doi.org/10.1016/j.ces.2013.11.009

# Experiments of mass transfer with liquid–liquid slug flow in square microchannels

N. Di Miceli Raimondi [a,b,*], L. Prat [a,b], C. Gourdon [a,b], J. Tasselli [c]

[a] Université de Toulouse, INPT, UPS, Laboratoire de Génie Chimique, 4, Allée Emile Monso, 31030 Toulouse, France
[b] CNRS, Laboratoire de Génie Chimique, 31030 Toulouse, France
[c] Laboratory for Analysis and Architecture of Systems, CNRS, 7 Avenue du Colonel Roche, 31077 Toulouse Cedex 4, France

## HIGHLIGHTS

- Experiments are carried out to study liquid–liquid mass transfer in microchannels.
- Solute concentration in the continuous phase is measured function of contact time.
- Droplet side mass transfer coefficients are identified from experimental results.
- The results are compared with models available in literature.

## ABSTRACT

Liquid–liquid mass transfer mechanism with slug flow in microreactor is investigated by means of experiments in square microchannels of 0.21 and 0.30 mm width. An experimental bench has been designed and an analytical protocol developed in order to follow the transfer of a solute from the dispersed phase to the continuous phase. The methodology used allows the identification of droplet side mass transfer coefficients. Total flow rate ranges from 5 to 50 mL $h^{-1}$, resulting in droplets velocities of 0.02–0.35 m $s^{-1}$. Volumetric mass transfer coefficient $k_d a$ values obtained in the present work ranges from 0.72 to 8.44 $s^{-1}$. The results reasonably fit with a model suggested by a previous study based on 2D direct numerical simulations. A comparison with other models available in the literature shows that in the operating conditions considered in this work, the flow pattern inside the confined droplets at microscale leads to an enhancement of mass transfer compared to droplets that are not confined.

*Keywords:*
Liquid–liquid mass transfer
Slug flow
Microchannel
Confined droplets

## 1. Introduction

Microreactors and microchannels are non-conventional devices in chemical engineering field but have been for few years the subject of numerous research studies and programs such as the European project IMPULSE (Integrated Multiscale Process Units with Locally Structured Elements) in 2005. This interest lies in the abilities of such devices in terms of heat transfer and mass transfer notably due to the increase of specific area by the miniaturization effect and the decrease of diffusion length. Ehrfeld et al. (2000) proposed a state of the art on microtechnologies: they observed that typical interfacial areas for two-phase flow are 5000–30,000 $m^2$ $m^{-3}$, while Kashid and Agar (2007) showed that the production130 of such dispersions requires low power input compared to common devices. Moreover, despite laminar flow, the confinement of two-phase flow in microchannels allows the appearance of recirculation vortices that can have positive effect on transfer mechanisms.

The use of miniaturized processes is promising according to two main frameworks: (i) process intensification (Stankiewicz and Moulijn, 2000; Commenge et al., 2005) with an improvement of safety due to confinement and small amount of chemicals (Burns and Ramshaw, 2001; De Mello and Wooton, 2002) and (ii) microdevices designed as labs on chips for data acquisition at laboratory scale such as kinetic data (Sarrazin, 2006; Tsoligkas et al., 2007), physico-chemical properties (Guillot et al., 2006) or biological mechanisms information (Stanley et al., 2012) for a better sizing and control of pilot and industrial plants. For both applications it is important to understand the physical and chemical mechanisms at microscale. To carry out liquid–liquid process, mass transfer coefficients estimation is required to obtain reliable process designs and/or data acquisitions for kinetic laws identification. Few works focused on experimental mass transfer

* Corresponding author at: Université de Toulouse, INPT, UPS, Laboratoire de Génie Chimique, 4, Allée Emile Monso, F-31030 Toulouse, France.
Tel.: +33 562 25 89 20; fax: +33 562 25 88 91.
*E-mail address:* nathalie.raimondi@iut-tlse3.fr (N. Di Miceli Raimondi).

with liquid–liquid slug flow in microchannels using reactive (with instantaneous reactions) or non-reactive systems. Burns and Ramshaw (2001) conducted experiments of acetic acid titration in kerosene within 0.38 mm width square microchannels. Dummann et al. (2003) carried out the nitration of single ring aromatics and Ghaini et al. (2010) used the alkaline hydrolysis of ester in *n*-butylformate in circular capillaries of 0.5 and 1 mm diameter. Dessimoz et al. (2008) worked in rectangular microchannels of 0.4 mm equivalent diameter and carried out the instantaneous neutralisation of trichloroacetic acid by NaOH in toluene or hexane. Assmann and von Rohr (2011) studied the extraction of vanillin in water with toluene with or without adding an inert gas in rectangular microchannels (173 μm × 300 μm). These works show an increase of the mass transfer coefficients with the droplets velocity (or total flow rate).

In a previous work based on 2D direct numerical simulations (Di Miceli Raimondi et al., 2008), a correlation has been proposed that shows the influence of the operating parameters on mass transfer coefficients. The present work consists in the development of a laboratory pilot and an analysis protocol to conduct liquid–liquid mass transfer experiments in square microchannels to validate this correlation and increase the comprehension of transfer mechanisms in such systems. Slug flow pattern is generated in T-shape microreactors. Transfer of acetone from toluene to water is carried out.

This article presents the materials used to carry out mass transfer experiments with liquid–liquid slug flow and the experimental protocol. The results obtained in terms of mass transfer coefficients on the droplet side are compared with the correlation suggested by the previous simulation work. Finally a comparison with models proposed for similar systems is conducted in order to understand the impact of the hydrodynamic structures in confined liquid–liquid slug flows on the mass transfer mechanism.

## 2. Materials

### 2.1. Microreactors

The experiments are carried out in two microreactors manufactured by the LAAS (Laboratory for Analysis and Architecture of Systems, CNRS Toulouse, France), whose main microchannels have square section of $0.21 \pm 0.01$ and $0.30 \pm 0.01$ mm width (Fig. 1). These ones are made of silicon and glass and present a very good chemical resistance.

The manufacturing of silicon microfluidic chips is achieved by means of the photolithography technique (Gawron et al., 2001; Chun et al., 2006). High-aspect-ratio microchannels are fabricated in a silicon wafer by plasma etching using the deep reactive ion etching (DRIE) technique and the Bosch process (Tang et al., 2007; Laermer and Schilp, 1996). Through-wafer holes are also etched by DRIE for creating the microreactor inlets and outlets. The structured silicon wafer is capped by a borosilicate glass wafer (Pyrex® 7740 from Corning) using anodic bonding technique. Resulting squared microchannels are made of three walls in silicon and one in glass.

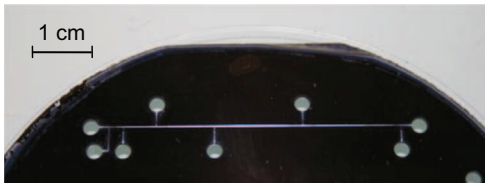


**Fig. 1.** Microreactor in silicium and glass.

Silicon and glass are hydrophilic so that the organic phase is dispersed into the aqueous phase. The fluids get in contact in a T-junction. Liquid–liquid slug flow is produced as illustrated in Fig. 2, with droplets and continuous phase slug that regularly alternates (a droplet and a continuous phase slug constitute a "unit cell").

The microreactors present secondary channels made of several small microchannels (20 μm width and 0.21 or 0.30 mm depth depending on the main channel size). They act like filters in order to extract in a selective way the continuous phase. This allows the analysis of the extracted fluid, i.e. the measurement of the solute concentration in the continuous phase (Fig. 3). Similar secondary channels have already been used for the management of dispersed flow pattern in microchannels (Gunther et al., 2005; Prat et al., 2006; Marcati et al., 2010).

### 2.2. Experimental bench

Fig. 3 presents a scheme of the experimental bench. The introduction of the fluids is performed by syringes with stainless steel needles placed on syringe pumps (Harvard Apparatus PHD2000 or PicoPlus). A high-speed camera HCC-1000 (VDS Vosskühler GmbH) coupled with a binocular Nikon SMZ-10 enables the visualization of the flow in the microchannel. The chip lighting is provided through optical beams. The camera is characterized by an acquisition frequency up to 1800 frames $s^{-1}$. Data acquisition and treatment is carried out using the software NV 1000 (New Vision Technologies). This system allows the measurement of the droplets length, velocity and frequency.

The analysis system is connected to one of the secondary channels to measure the solute concentration in the continuous phase at a given location. The others are blocked using plugged capillaries. The measuring system and the analytical method will be described in more details in Section 3.1.

### 2.3. Microfluidic connections

Silicon and glass are tough materials but highly breakable. Therefore, the microfluidic connection system with such chips is not trivial. The fragility of the materials prohibits the use of connections directly screwed on the chip. Moreover stuck connections are excluded because of the use of solvents. Tight microfluidic connections were obtained using silicon septa. As described on Fig. 4, a PFA (perfluoroalcoxy polymer, 1/16″ OD) capillary passes through a septum placed on each inlet and outlet. The septa and the microfluidic chip are put between two PMMA (polymethylmethacrylate) plates screwed each other to constitute the

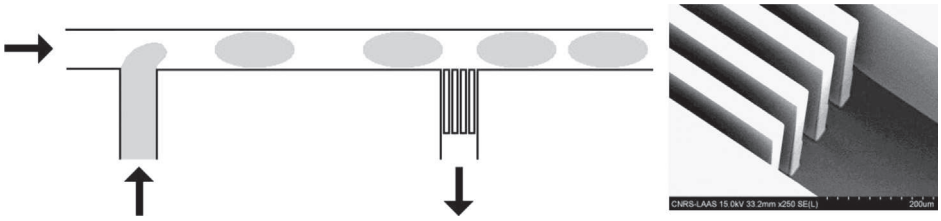

**Fig. 2.** Illustration of the microreactor structure (main and secondary channels).

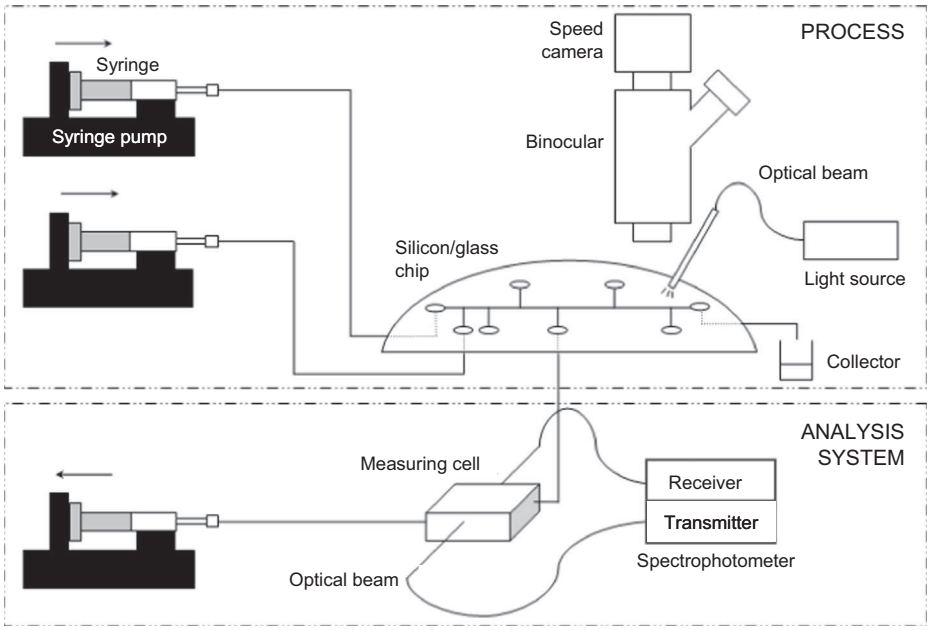


**Fig. 3.** Scheme of the experimental bench.

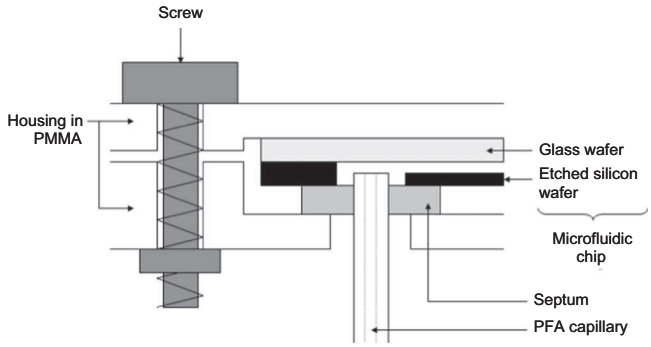


**Fig. 4.** Scheme of a microfluidic connection.

housing. The screwing allows the septa to be flattened against the silicium wafer. This provides a good tightening of the connection while applying a soft mechanical pressure on the chip. At last, connections between PFA capillaries and stainless steel needles are insured using Swagelok fittings.

## 3. Methods

### 3.1. Analytical method

Water/acetone/toluene two-phase system was used to characterize mass transfer in square microchannels. It is defined as a standard test system for liquid extraction by the European Federation of Chemical Engineering (Misek et al., 1985). Acetone is the solute which transfers from toluene (dispersed phase) to water (continuous phase).

As previously described, the concentration of acetone in the continuous phase is determined using secondary channels to extract this phase. For that purpose, the secondary channel which is subjected to analysis is linked to a syringe (by means of capillaries) which is placed on a syringe-pump running in refill mode (Fig. 3). In order to analyze continuous phase samples representative of this phase in the microchannel, half of its flow rate is constantly extracted. There are five secondary channels per microreactor located at a distance of 2.4 mm, 7.8 mm, 17.6 mm, 32.2 mm and 48.8 mm from the middle of the T-shape droplets generator. The total length of the main channel in which mass transfer occurs is 50.6 mm (from the droplets generator to the main outlet). The concentration of acetone in the continuous phase is determined by UV-spectrophotometry measurements. A measuring cell is placed between the secondary channel and the refill syringe as described in Fig. 5. The extracted fluid circulates in the cell while it is analyzed by mean of two optical beams (one acts like a light transmitter, the other like a receiver). This material allows the estimation of the fluid absorbance which can be directly linked to the concentration of acetone thanks to a prior calibration of the system with an uncertainty of 10%. The beams are connected to the spectrophotometer (AvaSpec-2048-USB2 Grating UA). The received signal is analyzed with the software Avasoft-Full.

Water and toluene are nearly mutually immiscible. However the very small solubility of toluene in water is enough to distort the measurement of acetone concentration in water (at ambient temperature, the solubility of toluene is roughly 0.5 g/L of water). This measurement allows the estimation of the solute flux transferred between the two phases. Therefore, to avoid the transfer of toluene and water, water saturated with toluene and toluene saturated with water have been used in the whole experiments performed at ambient temperature. Acetone concentrations are low in order to avoid a flow hydrodynamic perturbation due to mass transfer notably linked to Marangoni effects. Moreover the calibration of the system showed a linear relationship between fluid absorbance and acetone concentration up to 0.4% in weight of acetone in water. In these conditions, the physical properties of the two phase system are assumed to remain constant during the experiments equal to those of pure water ($\rho_c = 1\ \mathrm{g\ cm^{-3}}$; $\mu_c = 1 \times e^{-3}$ Pa s) and pure toluene ($\rho_d = 0.864\ \mathrm{g\ cm^{-3}}$; $\mu_d = 0.6 \times e^{-3}$ Pa s). Viscosity is measured with the rheometer CSL2 500 (TA Instruments). Density is measured with the pycnometer DMA 38 (Anton Paar). The interfacial tension between water and toluene is determined using the tensiometer 3S (GBX Instruments) at 33.7 mN $\mathrm{m^{-1}}$.

### 3.2. Experimental protocol

The continuous and dispersed phases flow rates, $Q_c$ and $Q_d$, are varied. For every operating conditions, the droplets length $L_d$, velocity $U_d$ and frequency $f_d$ are measured. Table 1 describes the

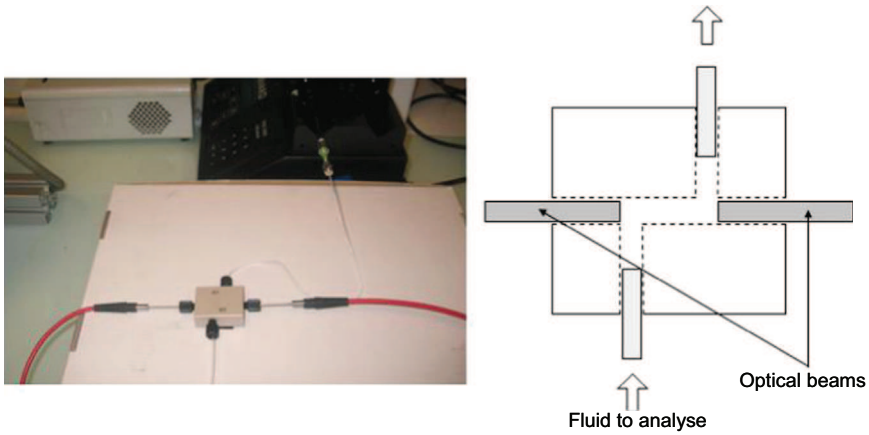


**Fig. 5.** Measuring cell associated to the UV-spectrophotometer.

**Table 1**
Operating conditions of the mass transfer experiments.

| $w_C$ (mm) | $Q_c$ (mL h$^{-1}$) | $Q_d$ (mL h$^{-1}$) | $L_d$ (mm) | $U_d$ (m s$^{-1}$) | $f_d$ (s$^{-1}$) | $k_{d,\exp}a$ (s$^{-1}$) | $a$ (m$^2$ m$^{-3}$) |
|---|---|---|---|---|---|---|---|
| 0.21 | 2.5 | 2.5 | 0.88 ± 0.04 | 0.030 ± 0.003 | 20.4 ± 3.7 | 1.61 ± 0.73 | 10 240 |
| 0.21 | 2.5 | 5.0 | 1.30 ± 0.12 | 0.044 ± 0.002 | 25.9 ± 2.8 | 2.72 ± 1.43 | 13 400 |
| 0.21 | 5.0 | 2.5 | 0.57 ± 0.02 | 0.045 ± 0.003 | 31.9 ± 2.9 | 1.53 ± 0.35 | 6 760 |
| 0.21 | 5.0 | 5.0 | 0.72 ± 0.06 | 0.060 ± 0.002 | 51.0 ± 3.7 | 3.58 ± 0.42 | 10 400 |
| 0.21 | 20.0 | 20.0 | 0.47 ± 0.03 | 0.270 ± 0.025 | 319.8 ± 12.0 | 8.44 ± 1.91 | 9 130 |
| 0.21 | 30.0 | 10.0 | 0.35 ± 0.02 | 0.266 ± 0.052 | 288.0 ± 11.5 | 4.33 ± 0.66 | 6 090 |
| 0.21 | 30.0 | 20.0 | 0.36 ± 0.04 | 0.347 ± 0.034 | 426.9 ± 21.4 | 8.43 ± 1.56 | 7 060 |
| 0.30 | 5.0 | 2.5 | 1.00 ± 0.11 | 0.025 ± 0.003 | 10.2 ± 0.7 | 1.06 ± 0.39 | 4 540 |
| 0.30 | 5.0 | 5.0 | 1.28 ± 0.14 | 0.034 ± 0.004 | 16.0 ± 0.9 | 1.23 ± 0.46 | 7 300 |
| 0.30 | 5.0 | 10.0 | 1.64 ± 0.18 | 0.052 ± 0.007 | 24.5 ± 3.7 | 0.72 ± 0.21 | 4 630 |
| 0.30 | 7.0 | 3.5 | 0.85 ± 0.06 | 0.036 ± 0.003 | 16.4 ± 1.0 | 1.53 ± 0.61 | 6 700 |
| 0.30 | 7.0 | 7.0 | 1.04 ± 0.15 | 0.049 ± 0.004 | 26.6 ± 2.9 | 2.65 ± 1.14 | 9 600 |
| 0.30 | 7.5 | 15.0 | 1.43 ± 0.19 | 0.077 ± 0.004 | 42.5 ± 3.4 | 1.18 ± 0.33 | 4 640 |
| 0.30 | 10.0 | 5.0 | 0.79 ± 0.04 | 0.052 ± 0.005 | 26.1 ± 1.5 | 1.85 ± 0.62 | 7 150 |
| 0.30 | 10.0 | 10.0 | 1.05 ± 0.07 | 0.070 ± 0.008 | 40.1 ± 2.8 | 1.45 ± 0.50 | 4 630 |
| 0.30 | 15.0 | 7.5 | 0.75 ± 0.03 | 0.079 ± 0.008 | 41.5 ± 1.9 | 2.20 ± 1.09 | 9 420 |

set of experiments carried out ($w_C$ stands for the microchannel width). The solute (acetone) is initially mixed in the dispersed phase (toluene). Its concentration $C_d^0$ is settled so that the concentration measurements are included in the range where concentration and absorbance of the analyzed solution are proportional. The continuous phase (water) is initially pure. Concentrations are expressed in acetone mass fraction. The method developed to measure the mass transfer coefficient $k_{d,\exp}a$ and the interfacial area $a$ is described in Section 4.

These experiments aim at estimating the droplet side mass transfer coefficient and identifying the impact of the dispersed flow characteristics on this coefficient. This requires deducing the impoverishment kinetics of the droplets in solute for every operating conditions investigated. The monitoring of the transfer all along the microchannel is achieved by connecting the measuring cell at the different secondary channels. The analysis method allows the measurement of the concentration of acetone in the continuous phase $C_c$. The concentration profile of acetone in the dispersed phase $C_d$ is then obtained with the following mass balance:

$$Q_d\rho_d C_d^0 = Q_d\rho_d C_d(t) + Q_c\rho_c C_c(t) \quad (1)$$

where $\rho$ is the fluid density, and $t$ is the residence time. It assumes that flow rates and densities of both phases remain constant during the transfer operation regarding the low concentrations of acetone used. Fig. 6 illustrates the curves trend obtained with such a protocol. The experimental error is estimated from the uncertainties on the droplets velocity, on the initial concentration of acetone in toluene and on the concentration of acetone measured by the spectrophotometry technique.

## 4. Results

### 4.1. Volumetric mass transfer coefficients identification

Droplet side mass transfer coefficient $k_{d,\exp}$ is identified from the experimental concentration profiles. It is derived from the expression of the mass flux through the interface per droplet surface unit $\Phi_{\exp}$ given by Eq. (2). The driving force is calculated from the difference between the concentration of acetone in the droplet at time $t$, $C_d(t)$, and the one at infinite time, $C_d^\infty$:

$$\Phi_{\exp} = -k_{d,\exp}(C_d(t) - C_d^\infty)\cdot\rho_d \quad (2)$$

$k_{d,\exp}$ is deduced from the experiments by fitting concentration profiles with those calculated by means of the mass balance within the droplets:

$$V_d\frac{dC_d(t)}{dt} = -k_{d,\exp}aV_{UC}(C_d(t) - C_d^\infty) \quad (3)$$

$a$ stands for the interfacial area of the two-phase flow. $V_d$ and $V_{UC}$ respectively represent the volumes of a droplet and a unit cell. A unit cell corresponds to the flow pattern which comprises a droplet and a continuous phase liquid slug. $V_{UC}$ is obtained from the product of the unit cell length $L_{UC}$ with the section of the main microchannel. The droplet volume $V_{d,\exp}$ corresponds to the ratio

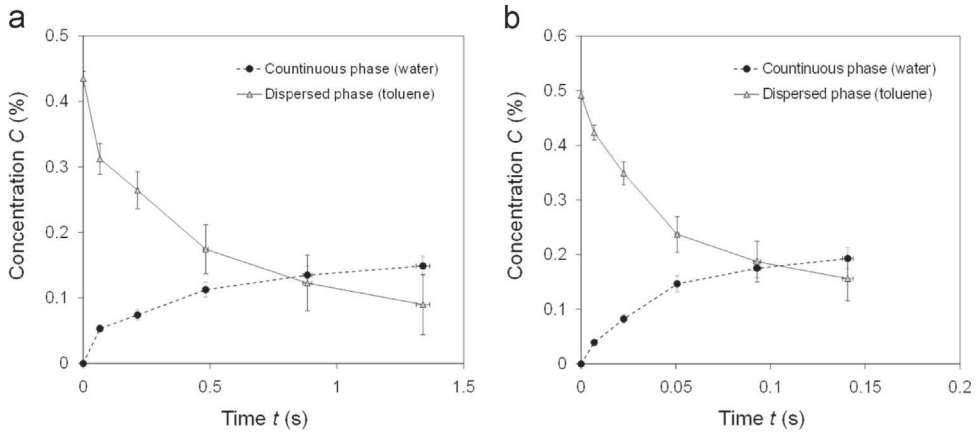


**Fig. 6.** Concentration profiles of acetone in the continuous phase (measured) and in the dispersed phase (calculated). (a) $w_C$=0.30 mm, $Q_c$=7 mL h$^{-1}$, $Q_d$=3.5 mL h$^{-1}$; (b) $w_C$=0.21 mm, $Q_c$=30 mL h$^{-1}$, $Q_d$=20 mL h$^{-1}$.

between the dispersed phase flow rate and the droplets frequency:

$$V_{d,\exp} = \frac{Q_d}{f_d} \tag{4}$$

The integration of the mass balance over time can be written as follows:

$$C_d(t) = C_d^{\infty} + (C_d(t_{ref}) - C_d^{\infty}) \exp\left( -\frac{k_{d,\exp} a V_{UC}}{V_{d,\exp}} (t - t_{ref}) \right) \tag{5}$$

$t_{ref}$ is a reference time from which it assumes that Eq. (2) can reliably predict mass transfer fluxes. The effect of the droplet formation generally leads to a global overestimation of mass transfer coefficients due to the appearance of mixing hydrodynamic structures when the phases get in contact. In this study, $t_{ref}$ was chosen in the zone where the laminar flow in the microchannel is fully developed in order to avoid the entrance effects impact on $k_{d,\exp}$ estimation (Skelland and Wellek, 1964). The entrance length $L^e$ considering laminar flow in smooth channel can be estimated using Eq. (6) (Gao et al., 2002; Shen et al., 2006):

$$\frac{L^e}{d_C \mathrm{Re}} = 0.1 \tag{6}$$

In the experiments carried out, the entrance length is evaluated to be less than 1.4 mm in the channel of 0.21 mm width, and 0.7 mm in the channel of 0.30 mm width. The first secondary channel is located at 2.4 mm from the T-junction. Therefore, it is expected that the flow is fully developed at that level of the main channel. Consequently, the time of reference $t_{ref}$ is defined as the time for a droplet to reach the first secondary channel. $C_d^{\infty}$ is calculated from a mass balance at infinite contact time given by Eq. (7):

$$C_d^0 \rho_d Q_d = C_d^{\infty} \rho_d Q_d + C_c^{\infty} \rho_c Q_c \tag{7}$$

$C_d^{\infty}$ and $C_c^{\infty}$ are linked together by the thermodynamic equilibrium. A prior study showed that this equilibrium can be written in terms of Eq. (8) in the concentration domain considered in this work, with a constant partition coefficient $m$=0.76.

$$C_d^{\infty} = m \cdot C_c^{\infty} \tag{8}$$

Therefore, Eqs. (7) and (8) allows the estimation of $C_d^{\infty}$:

$$C_d^{\infty} = C_d^0 \frac{\rho_d Q_d}{\rho_d Q_d + \rho_c Q_c / m} \tag{9}$$

By fitting Eq. (5) to the experimental profiles, coefficient ($k_{d,\exp} a \cdot V_{UC}/V_d$) can be identified for the whole experiments. Fig. 7 illustrates the result of the fitting for some of the experiments. A satisfactory representation of the experimental data is observed (the initial point is not taken into account as explained before because of the mass transfer overestimation due to the droplet generation).

Volumetric mass transfer coefficient in terms of $k_{d,\exp}a$ product ranges from 0.72 to 8.44 s$^{-1}$. The higher values are obtained for the higher droplets velocities, around 0.3 m s$^{-1}$, while most of the values are of the order of magnitude of 2 s$^{-1}$ for droplets velocity ranging from 0.025 to 0.08 m s$^{-1}$.

Table 2 presents the results of other authors: Ghaini et al. (2010) and Assmann and von Rohr (2011) considered the global mass transfer coefficient while the present work and Dessimoz et al.'s (2008) study are focusing on droplet side mass transfer coefficient. Assmann and von Rohr carried out experiments with similar flow velocity range (0.04–0.3 m s$^{-1}$) and hydraulic diameter. Their $k_La$ values are close to those observed in the present study. The values presented by Ghaini et al. are consistent with the present work considering the fact that these authors used capillaries with diameter higher than the width of the square microchannel used in the present study (0.5–1 mm vs. 0.21–0.30 mm). Finally, Dessimoz et al. obtained lower values of mass transfer coefficients (around 10 times lower) but they worked with lower droplets velocity (0–0.02 m s$^{-1}$).

The interfacial area estimated in the present work is related to the entire surface of the droplets while Ghaini et al. (2010) measured it using a chemical method. They showed that depending on the operating conditions (notably the slug velocity), the interfacial area can be estimated from the droplet surface with or without considering the surface in contact with the film between the droplet and the channel wall. This can be explained by the saturation time of the film that can be significantly lower than the saturation time of the continuous phase slug, function of the dispersed flow characteristics.

### 4.2. Interfacial area modeling

The interfacial area of the two-phase flow $a$ is estimated as a function of the droplets shape. It is assumed that this parameter depends on the capillary number $\mathrm{Ca}_d$ (Kreutzer et al., 2005) defined in terms of Eq. (10):

$$\mathrm{Ca}_d = \frac{\mu_c U_d}{\sigma} \tag{10}$$

where $\mu_c$ is the viscosity of the continuous phase and $\sigma$ the interfacial tension of the liquid–liquid system. Kreutzer et al. (2005) suggested that:

- $\mathrm{Ca}_d \geq 0.04$: the droplet section is axisymmetric. Its body shape can be assimilated to a cylinder, with a diameter $w_d$ given by

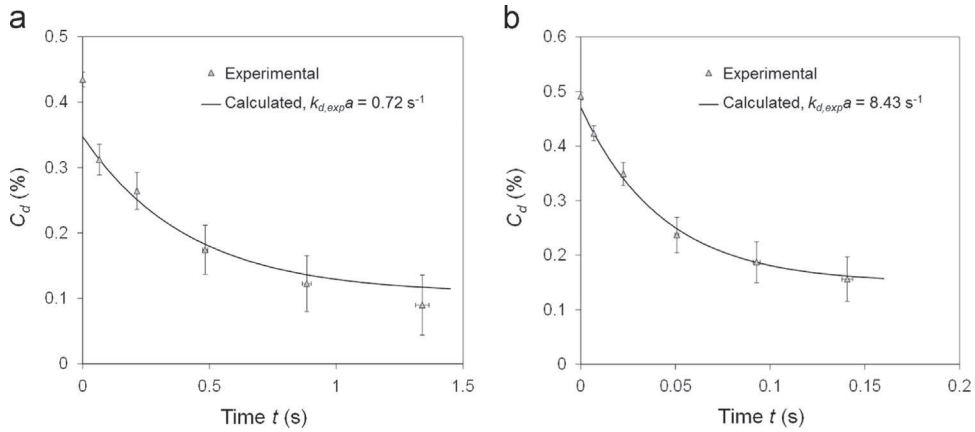


**Fig. 7.** Comparison between experimental and calculated (Eq. (5)) concentration profiles in the dispersed phase. (a) $w_C$=0.30 mm, $Q_c$=7 mL h$^{-1}$, $Q_d$=3.5 mL h$^{-1}$; (b) $w_C$=0.21 mm, $Q_c$=30 mL h$^{-1}$, $Q_d$=20 mL h$^{-1}$.

**Table 2**
Liquid–liquid mass transfer coefficients and interfacial area in microreactor.

| Liquid–liquid contactor | $k_La$ or $k_da$ (s$^{-1}$) | $a$ (m$^2$ m$^{-3}$) | Reference |
|---|---|---|---|
| Square microchannel, $w_C$=0.21 mm | 1.61–8.44 | 6090–13400 | Present work |
| Square microchannel, $w_C$=0.30 mm | 0.72–2.65 | 4540–9600 | Present work |
| Rectangular microchannel, $d_H$=0.22 mm | 5–12 | – | Assmann and von Rohr (2011) |
| Rectangular microchannel, $d_H$=0.4 mm | 0.2–0.5 | ~10,000 | Dessimoz et al. (2008) |
| Capillary microreactor, ID=0.5 mm | 0.90–1.67 | 1600–3200 | Ghaini et al. (2010) |
| Capillary microreactor, ID=0.75 mm | 0.91–1.46 | 1075–2770 | Ghaini et al. (2010) |
| Capillary microreactor, ID=1 mm | 0.88–1.29 | 830–2480 | Ghaini et al. (2010) |

the following correlation ($w_C$ refers to the channel width):

$$\frac{w_d}{w_C} = 0.7 + 0.5\exp(-2.25\mathrm{Ca}_d^{0.445}) \quad (11)$$

- $\mathrm{Ca}_d < 0.04$: the droplet body fits the channel walls very closely. Its section can be assimilated to the channel section, i.e. as a square, with a width equal to $0.95w_C$.

The droplet ends are assimilated to hemispheres. In the experiments carried out, $\mathrm{Ca}_d$ ranges from 0.001 to 0.01 ($\mathrm{Ca}_d <$ 0.04). In order to validate the shape model, the calculated droplets volume (given by Eq. (12)) is compared to the experimental one (Eq. (4)). Fig. 8 shows a good agreement between both of them:

$$V_{d,calc} = \frac{\pi w_d^3}{6} + w_d^2(L_d - w_d) \quad \text{for } \mathrm{Ca}_d < 0.04 \quad (12)$$

Therefore, the surface of one droplet $S_d$ is estimated from the following:

$$S_d = \pi w_d^2 + 4w_d(L_d - w_d) \quad \text{for } \mathrm{Ca}_d < 0.04 \quad (13)$$

The interfacial area of the liquid–liquid system $a$ is defined as the ratio between the surface of one droplet and the unit cell volume (given by the following):

$$a = \frac{S_d}{L_{UC} \cdot {d_C}^2} \quad (14)$$

In this work, it ranges from 4540 to 13,400 m$^2$ m$^{-3}$. Consequently, the $k_{d,\mathrm{exp}}a$ values previously identified allows the estimation of the mass transfer coefficient $k_{d,\mathrm{exp}}$ that ranges from 1.5e−04 to 1.4e−03 m s$^{-1}$. Fig. 9 shows that, as expected, the mass transfer coefficient tends to increase with the droplets velocity. The error bars represent the uncertainties on the measured values given in Table 1.

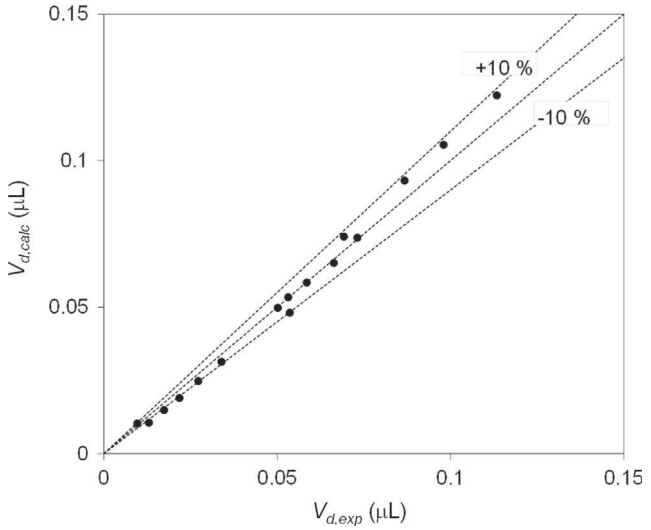


**Fig. 8.** Comparison between calculated (Eq. (12)) and experimental (Eq. (9)) droplet volume.

## 5. Comparison with models for mass transfer coefficient estimation

### 5.1. Validation of a previous numerical study

In a previous work, a correlation for the estimation of droplet side mass transfer coefficient has been proposed for liquid–liquid mass transfer with slug flow as a function of the flow characteristics (Di Miceli Raimondi et al., 2008). It is based on 2D direct numerical simulations. The correlation is as follows:

$$k_d d_d = \alpha \cdot \left(\frac{V_d}{V_{UC}}\right)^{0.17} (U_d w_C)^{0.69} \left(\frac{U_d}{\sigma}\right)^{-0.07} \left(\frac{w_C}{d_d}\right)^{0.75} \quad (15)$$

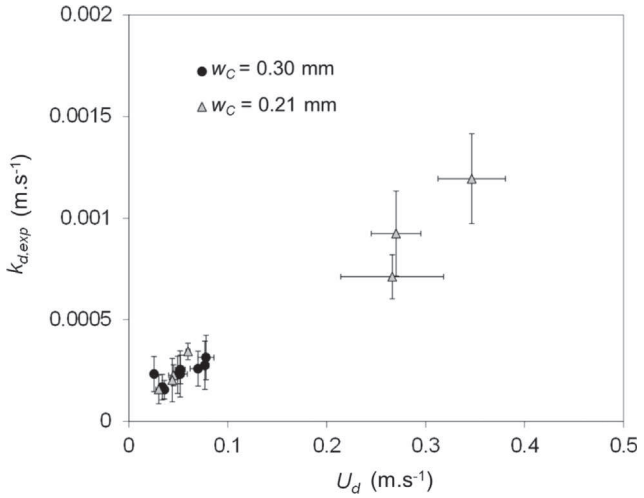


**Fig. 9.** Mass transfer coefficient in function of droplets velocity.

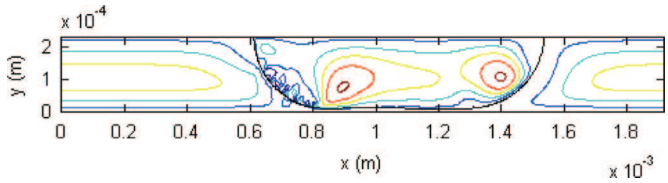


**Fig. 10.** Flow structure observed for confined droplets at low capillary number (Di Miceli Raimondi et al., 2008).

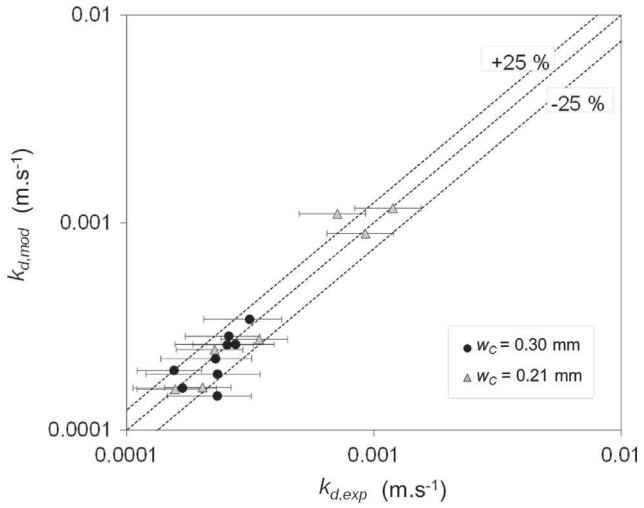


**Fig. 11.** Comparison between experimental and calculated mass transfer coefficients (Eq. (14)).

where $d_d$ is the droplet equivalent diameter (diameter of a spherical droplet with the same volume). $\alpha$ is a constant that depends on the fluid properties and the flow characteristics inside the droplets differentiated according to the flow structures type inside the droplets. In the present work, capillary number is low and the droplets are highly confined resulting in flow patterns with numerous vortices as illustrated by Fig. 10. Indeed $Ca_d$ ranges from 0.0007 to 0.0103 and $L_d/w_C$ from 1.7 to 6.6. In this particular case, it leads to $\alpha$=4.36e−04.

As illustrated in Fig. 11, mass transfer coefficients obtained in the present experimental study are well estimated by Eq. (14). The maximal relative error between the model and the experiments observed is 55% and the median relative error is about 10%.

## 5.2. Comparison with literature

### 5.2.1. Mass transfer models description

Mass transfer models proposed in literature for systems approaching liquid–liquid slug flow are described afterwards.

*5.2.1.1. Dispersed liquid–liquid systems in infinite media.* Numerous empirical models are available (Knudsen et al., 1998; Slater, 1994). Skelland and Wellek correlation seems appropriate for comparison with experiments in microchannels since they developed a model for circulating droplets, i.e. with internal recirculation loops and a non-oscillating interface which is close from the flow structures observed with liquid–liquid slug flow in microdevices (Harries et al., 2003; Sarrazin et al., 2008; Kashid et al., 2008). This model is given by Eq. (15). Mass transfer coefficient depends on Fourier number defined as a function of the exposure time $t_e$ and the diffusion time. The exposure time is estimated using Eq. (16) assuming that the contact length corresponds to the length traveled by a fluid element by convection at the droplets interface at the interface velocity, i.e. the droplet velocity. The diffusion time is related to the diffusivity of the solute in the dispersed phase $D_d$ and the characteristic length of diffusion in this phase, assumed to be equal to half the equivalent diameter of the droplet:

$$\frac{k_d d_d}{D_d} = 31.4\left(\frac{\rho_c U_d d_d}{\mu_c}\right)^{0.371}\left(\frac{\mu_c U_d}{\sigma}\right)^{0.371}\left(\frac{4D_d}{t_e {d_d}^2}\right)^{-0.338}\left(\frac{\mu_d}{\rho_d D_d}\right)^{-0.125} \tag{16}$$

$$t_e = \frac{(L_d - w_d) + \pi w_d/2}{U_d} \tag{17}$$

The diffusion coefficient of acetone in toluene in highly diluted solutions at ambient temperature is estimated at 2.8e−09 m$^2$ s$^{-1}$ (Bulicka and Prochazka, 1976).

*5.2.1.2. Gas–liquid Taylor flow at microscale.* Gas–liquid two-phase flow in microchannels has been recently intensely investigated, notably in Taylor flow regime. This interest is notably due to the diversity of potential applications for these systems (miniaturization of chemical processes for safety and/or heat and mass transfer enhancement, biotechnology systems, space applications, etc.). Several authors proposed models to predict mass transfer coefficients in such two-phase flow (Bercic and Pintar, 1997; Irandoust et al., 1992; Kreutzer, 2003; Van Baten and Krishna, 2004; Vandu et al., 2005; Yue et al., 2007; Liu and Wang, 2011). Shao et al. (2010) compared most of these models with their own mass transfer coefficients obtained by computational fluid dynamics simulations. They observed three tendencies: (i) models based on mass transfer contributions from both bubble caps and film between the bubble and the wall tend to overestimate their values (van ); (ii) models where only the film contributes to mass transfer give reasonable predictions (Vandu et al., 2005); and (iii) models where only the bubble caps contribute to mass transfer tend to underestimate their values. These models were established under conditions where the film quickly saturates because of large bubble lengths (Bercic and Pintar, 1997) or high bubble velocities (Yue et al., 2007).

In order to compare mass transfer mechanisms in gas–liquid flow and in liquid–liquid slug flow, three models are considered:

- Van Baten and Krishna (2004) model which considers that the entire bubble surface contributes to mass transfer. They express mass transfer coefficient as the sum of two contributions given by Eq. (17). Bubble caps contribution is estimated according to Higbie penetration theory Eq. (18). The term related to the

transfer through the film is obtained by referring to the model of mass transfer from a bubble to a laminar falling film, as a function of Fourier number (Eqs. (19)–(22)). This number is relevant for the saturation rate of the film (Pohorecki, 2007). In the experiments, the Fourier number ranges from 0.02 to 1.1. The formulation given by Eq. (20) has been privileged for $Fo < 0.1$; Eq. (21) for $Fo > 0.1$. The film thickness $\delta_{film}$ can be estimated at $0.025\, w_C$ for $Ca < 0.04$ (Kreutzer et al., 2005). $D_c$ corresponds to the diffusion coefficient of acetone in water in dilute solution at ambient temperature, equal to $1.2e-09\ m^2\ s^{-1}$ (Grossmann and Winkelmann, 2005):

$$k_L a = k_{L,cap} a_{cap} + k_{L,film} a_{film} \tag{18}$$

$$k_{L,cap} a_{cap} = \left(\frac{2\sqrt{2}}{\pi}\sqrt{\frac{D_c U_d}{w_d}}\right)\left(\frac{\pi w_d^2}{L_{UC} w_C^2}\right) \tag{19}$$

$$Fo_{film} = \frac{D_c L_{film}}{U_d \delta_{film}^2} \tag{20}$$

$$k_{L,film} a_{film} = \left(2\sqrt{\frac{D_c U_d}{\pi(L_d - w_d)}\frac{\ln(1/\Delta)}{1-\Delta}}\right)\left(\frac{4 w_d (L_d - w_d)}{L_{UC} w_C^2}\right) \quad \text{for } Fo_{film} < 0.1 \tag{21}$$

$$k_{L,film} a_{film} = \left(3.41\frac{D_c}{\delta_{film}}\right)\left(\frac{4 w_d (L_d - w_d)}{L_{UC} w_C^2}\right) \quad \text{for } Fo_{film} > 1 \tag{21}$$

$$\Delta = 0.7857\exp(-5.121 Fo_{film}) + 0.1001\exp(-39.21 Fo_{film}) + 0.0360\exp(-105.6 Fo_{film}) \pm 0.04 \tag{22}$$

- Van Baten and Krishna (2004) model where only the film contribution is taken into account.
- Bercic and Pintar (1997) model where only the bubble caps contribution is taken into account because of fast film saturation:

$$k_L a = \frac{0.111 U_d^{1.19}}{((1-\varepsilon_d) L_{UC})^{0.57}} \tag{23}$$

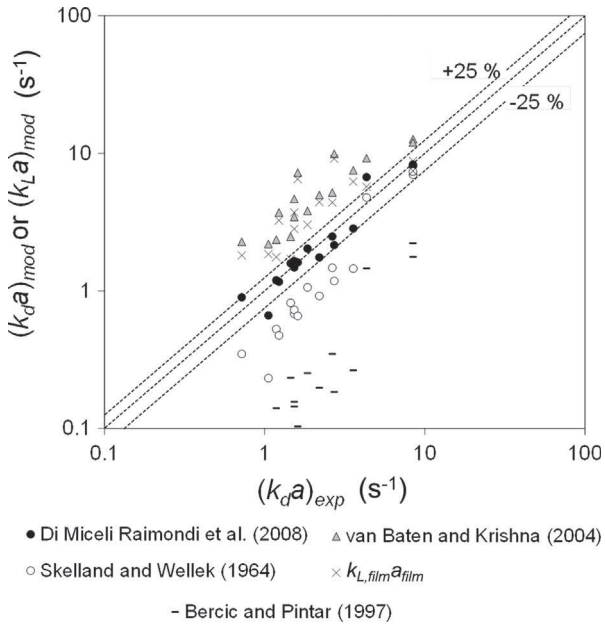


**Fig. 12.** Comparison between experimental results and models.

*5.2.2. Comparison of experimental volumetric mass transfer coefficient with models*

Fig. 12 shows the comparison between our experimental results obtained for liquid–liquid slug flow in square microchannels and the different models described above.

Concerning the models established for gas–liquid mass transfer in microchannels, Bercic and Pintar model underestimates the experimental results (90% of relative error). Film saturation is not quickly achieved: this is consistent with Fourier number values that are lower than 1. Van Baten and Krishna and film models overestimate the experiments. Mixing in bubbles is more intense than in confined droplets. The resistance in the dispersed phase to transfer that is neglected in gas–liquid Taylor flow limits the reliability of the gas–liquid models to predict liquid–liquid mass transfer.

Skelland and Wellek model underestimates the experiments with a mean relative error of 50%. It may be more appropriate to represent mass transfer with microfluidic flow patterns where droplets are not confined. Indeed, their model gives reasonable estimation of the experimental data for the higher values of $k_d a$ where the droplets confinement is minimal ($L_d/w_C = 1.77$–$2.35$). Therefore, it appears that confinement is favorable to mass transfer thanks to the appearance of mixing flow structures inside the droplets.

## 6. Conclusions

Liquid–liquid mass transfer experiments have been carried out in square microchannels of 0.21–0.30 mm width. The microreactor is composed of a main channel where the transfer operates and secondary channels that allows the selective extraction of the continuous phase for analysis. The pilot and the analytical method used enable to follow the enrichment of the continuous phase (water) in solute (acetone). The concentration profile of solute in the dispersed phase (toluene) all along the microchannel is obtained by mass balance from which a droplet side mass transfer coefficient is identified. The experimental results validate the correlation for mass transfer coefficients estimation for liquid–liquid slug flow in microchannels issued in a previous work from 2D direct numerical simulations.

In order to understand the transfer mechanism in the studied system, the experimental results are compared with models available in literature: liquid–liquid mass transfer in recirculating drops with non-oscillating interface in channel of conventional size and gas–liquid mass transfer in microchannels with Taylor flow pattern. The comparison shows that when the flow structure in the droplets presents numerous vortices ($Ca_d < 0.01$, $L_d/w_C > 1$), the droplets have a behavior intermediate between bubbles with high mixing rate in the gas phase and droplets that are not confined by the channel walls, the confinement being a factor of enhancement of mass transfer thanks to the appearance of recirculation flow structures.

This work could be completed by carrying out experiments with different flow pattern inside the droplets. Moreover the operating temperature and/or the fluids should be modified in order to investigate the influence of the fluids physical properties on mass transfer.

## Nomenclature

| | |
|---|---|
| $a$ | interfacial area ($m^2\ m^{-3}$) |
| $C$ | concentration in terms of mass fraction (kg of solute $kg^{-1}$ of phase) |
| Ca | Capillary number |

| | |
|---|---|
| $d_d$ | droplet equivalent diameter (m) |
| $d_H$ | channel hydraulic diameter (m) |
| $D$ | diffusion coefficient (m $s^{-2}$) |
| $f$ | frequency ($s^{-1}$) |
| Fo | Fourier number |
| $k$ | mass transfer coefficient (m $s^{-1}$) |
| $L$ | length (m) |
| $m$ | equilibrium constant |
| $Q$ | volumetric flow rate ($m^3$ $s^{-1}$) |
| $S$ | surface ($m^2$) |
| $t$ | residence time (s) |
| $t_e$ | exposure time (s) |
| $U$ | velocity (m $s^{-1}$) |
| $V$ | volume ($m^3$) |
| $w$ | width (m) |

*Greek letters*

| | |
|---|---|
| $\delta$ | thickness (m) |
| $\Delta$ | parameter defined by Eq. (22) |
| $\mu$ | dynamic viscosity (Pa s) |
| $\rho$ | density (kg $m^{-3}$) |
| $\sigma$ | interfacial tension (N $m^{-1}$) |
| $\Phi$ | mass flux by droplet surface unit (kg $s^{-1}$ $m^{-2}$) |

*Subscripts*

| | |
|---|---|
| $c$ | continuous phase |
| $C$ | channel |
| *calc* | calculated |
| *cap* | refers to the droplets caps |
| $d$ | dispersed phase or droplets |
| exp | refers to experimental data |
| *film* | refers to the film |
| $L$ | liquid phase |
| *mod* | estimated with a mass transfer coefficient model |
| *ref* | at time of reference |

*Superscripts*

| | |
|---|---|
| 0 | at inlet |
| $\infty$ | at thermodynamic equilibrium |

## Acknowledgments

This work has been supported by the 6th Framework EU under Grant IMPULSE no NMP2-CT-2005–011816 and the Institut National Polytechnique of Toulouse. Other contributing partners are CNRS, the University of Toulouse and LAAS.

## References

Assmann, N., von Rohr, P.R., 2011. Extraction in microreactors: intensification by adding an inert gas phase. Chem. Eng. Proc. Process Intensification 50, 822–827.
Bercic, G., Pintar, A, 1997. The role of gas bubbles and liquid slug lengths on mass transport in the Taylor flow through capillaries. Chem. Eng. Sci. 52 (21–22), 3709–3719.
Bulicka, J., Prochazka, J., 1976. Diffusion coefficients in some ternary systems. J. Chem. Eng. Data 21 (4), 452–456.
Burns, J.R., Ramshaw, C., 2001. The intensification of rapid reactions in multiphase systems using slug flow in capillaries. Lab Chip 1, 10–15.
Chun, M.-S., Shim, M.S., Choi, N.W., 2006. Fabrication and validation of a multi-channel type microfluidic chip for electrokinetic streaming potential devices. Lab Chip 6, 302–309.
Commenge, J.M., Falk, L., Corriou, J.P., Matlosz, M., 2005. Analysis of microstructured reactor characteristics for process miniaturization and intensification. Chem. Eng. Technol. 28 (4), 446–458.
De Mello, A., Wooton, R., 2002. But what is it good for? Applications of microreactor technology for the fine chemical industry. Lab Chip 2, 7N–13N.
Dessimoz, A.L., Cavin, L., Renken, A., Kiwi-Minsker, L., 2008. Liquid–liquid two-phase flow patterns and mass transfer characteristics in rectangular glass microreactors. Chem. Eng. Sci. 63, 4035–4044.
Di Miceli Raimondi, N., Prat, L., Gourdon, C., Cognet, P., 2008. Direct numerical simulations of mass transfer in square microchannels for liquid–liquid slug flow. Chem. Eng. Sci. 63, 5522–5530.
Dummann, G., Quittmann, U., Groschel, L., Agar, D.W., Worz, O., Morgenschweis, K., 2003. The capillary-microreactor: a new reactor concept for the intensification of heat and mass transfer in liquid–liquid reactions. Catal. Today 79–80, 433–439.
Ehrfeld, W., Hessel, V., Lowe, H., 2000. State of the art of microreaction technology, Microreactors: New Technology for Modern Chemistry. Wiley-VCH, Weinheim, pp. 1–14.
Gao, P., Le Person, S., Favre-Marinet, M., 2002. Scale effects on hydrodynamics and heat transfer in two-dimensional mini and microchannels. Int. J. Therm. Sci. 41, 1017–1027.
Gawron, A.J., Scott Martin, R., Lunte, S.M., 2001. Microchip electrophoretic separation systems for biomedical and pharmaceutical analysis. Eur. J. Pharm. Sci. 14, 1–12.
Ghaini, A., Kashid, M.N., Agar, D.W., 2010. Effective interfacial area for mass transfer in the liquid–liquid slug flow capillary microreactors. Chem. Eng. Proc. Process Intensification 49, 358–366.
Grossmann, T., Winkelmann, J., 2005. Ternary diffusion coefficients of glycerol+acetone+water by Taylor dispersion measurements at 298.15 K. J. Chem. Eng. Data 50, 1396–1403.
Guillot, P., Panizza, P., Salmon, J.B., Joanicot, M., Colin, A., Bruneau, C.H., Colin, T., 2006. Viscosimeter on a microfluidic chip. Langmuir 22, 6438–6445.
Gunther, A., Jhunjhunwala, M., Thalmann, M., Schmidt, M.A., Jensen, K.F., 2005. Micromixing of miscible liquids in segmented gas–liquid flow. Langmuir 21, 1547–1555.
Harries, N., Burns, J.R., Barrow, D.A., Ramshaw, C., 2003. A numerical model for segmented flow in a microreactor. Int. J. Heat Mass Transfer 46, 3313–3322.
Irandoust, S., Ertlé, S., Andersson, B., 1992. Gas–liquid mass transfer in Taylor flow through a capillary. Can. J. Chem. Eng. 70, 115–119.
Kashid, M.N., Agar, D.W., 2007. Hydrodynamics of liquid–liquid slug flow capillary microreactor: flow regimes, slug size and pressure drop. Chem. Eng. J. 131, 1–13.
Kashid, M.N., Fernandez Rivas, D., Agar, D.W., Turek, S., 2008. On the hydrodynamics of liquid–liquid slug flow capillary microreactors Asia-Pac. J. Chem. Eng. 3, 150–160.
Knudsen, J.G., Hottel, H.C., Sarofim, A.F., Wankat, P.C., Knaebel, K.S., 1998. Heat and mass transfer. In: Perry, R.H., Green, D.W. (Eds.), Perry's Chemical Engineer's Handbook, 7th ed. McGraw-Hill, New York.
Kreutzer, M.T., 2003. Hydrodynamics of Taylor Flow in Capillaries and Monolith Reactors. Ph.D. Thesis. Delft University of Technology, Delft, The Netherlands.
Kreutzer, M.T., Kapteijn, F., Moulijn, J.A., Heiszwolf, J.J., 2005. Multiphase monolith reactors: chemical reaction engineering of segmented flow in microchannels. Chem. Eng. Sci. 60, 5895–5916.
Laermer, F., Schilp, A., 1996. Method of anisotropically etching silicon, U.S. Patent 5501893.
Liu, D., Wang, S., 2011. Gas–liquid mass transfer in Taylor flow through circular capillaries. Ind. Eng. Chem. Res. 50, 2323–2330.
Marcati, A., Serra, C., Bouquey, M., Prat, L., 2010. Handling of polymer particles in microchannels. Chem. Eng. Technol. 33, 1779–1787.
Misek, T., Berger, R., Schröter, J., 1985. Standard Test Systems for Liquid Extraction. The Institution of Chemical Engineers, Rugby, England.
Pohorecki, R., 2007. Effectiveness of interfacial area for mass transfer in two-phase flow in microreactors. Chem. Eng. Sci. 62, 6495–6498.
Prat, L.E., Sarrazin, F., Tasseli, J., Marty, A., 2006. Increasing and decreasing droplets velocity in micro channels. Microfluidics Nanofluidics 2, 271–274.
Sarrazin, F., 2006. Microréacteurs diphasiques pour le développement rapide des procédés. Ph.D. Thesis. University of Toulouse, Toulouse, France.
Sarrazin, F., Bonometti, T., Prat, L., Gourdon, C., Magnaudet, J., 2008. Hydrodynamic structures of droplets engineered in rectangular micro-channels. Microfluidics Nanofluidics 5 (1), 131–135.
Shen, S., Xu, J.L., Zhou, J.J., Chen, Y., 2006. Flow and heat transfer in microchannels with rough wall surface. Energy Convers. Manage. 47, 1311–1325.
Shao, N., Gavriilidis, A., Angeli, P., 2010. Mass transfer during Taylor flow in microchannels with and without chemical reaction. Chem. Eng. J. 160, 873–881.
Skelland, A.H.P., Wellek, R.M., 1964. Resistance to mass transfer inside droplets. AIChE J. 10 (4), 491–496.
Stanley, C.E., Wootton, R.C.R, de Mello, A.J., 2012. Continuous and segmented flow microfluidics: applications in high-throughput chemistry and biology. Chimia 66, 88–98.
Slater, M.J., 1994. Rate coefficients in liquid–liquid extraction systems. In: Godfrey, J.C., Slater, M.J. (Eds.), Liquid–Liquid Extraction Equipment. Wiley, New York, pp. 45–94.
Stankiewicz, A.I., Moulijn, J.A., 2000. Process intensification: transforming chemical engineering. Chem. Eng. Prog. 96 (1), 22–34.
Tang, M., Liu, A.Q., Agarwal, A., Habib, M.H., 2007. A single-mask substrate transfer technique for the fabrication of high-aspect-ratio micromachined structures. J. Micromech. Microeng. 17, 1575–1582.

Tsoligkas, A.N., Simmons, M.J.H., Wood, J., Frost, C.G., 2007. Kinetic and selectivity studies of gas–liquid reaction under Taylor flow in a circular capillary. Catal. Today 128, 36–46.
Van Baten, J.M., Krishna, R., 2004. CFD simulations of mass transfer from Taylor bubbles rising in circular capillaries. Chem. Eng. Sci. 59, 2535–2545.
Vandu, C.O., Liu, H., Krishna, R., 2005. Mass transfer from Taylor bubbles rising in single capillaries. Chem. Eng. Process. 60, 6430–6437.
Yue, J., Chen, G., Yuan, Q., Luo, l., Gonthier, Y., 2007. Hydrodynamics and mass transfer characteristics in gas–liquid flow through a rectangular microchannel. Chem. Eng. Sci. 62, 2096–2108.